Exploiting Cherenkov Radiation With BGO-Based Metascintillators

Riccardo Latella, Antonio J. Gonzalez, *Member, IEEE*, Daniel A. B. Bonifacio, Miroslavna Kovylina, Amadeu Griol, José M. Benlloch, Paul Lecoq, *Fellow, IEEE*, and Georgios Konstantinou, *Member, IEEE*

***Abstract*—In time-of-flight positron emission tomography (TOF-PET), the timing capabilities of the scintillation-based detector play an important role. An approach for fast timing is using the so-called metascintillators, which combine two materials leading to the synergistic blending of their favorable characteristics. An added effect for BGO-based metascintillators is taking advantage of better transportation of Cherenkov photons through UV-transparent materials such as plastic (type EJ232). To prove this, we use an optimized Coincidence Time Resolution (CTR) setup based on electronic boards with two output signals (timing and energy) and near-ultraviolet (NUV) and vacuum-ultraviolet (VUV) silicon photomultipliers (SiPMs) from Fondazione Bruno Kessler (FBK), along with different coupling materials. As a reference detector, we employed a 3×3×5-mm^3 LYSO:Ce,Ca crystal pixel coupled with optical grease to an NUV-HD SiPM. The evaluation is based on low-threshold rise time, energy and time of arrival of event datasets. Timing results of a BGO/EJ232 3×3×15-mm^3 metapixel show detector time resolutions (DTRs) of 159 ps for the full photopeak. We demonstrate the possibility of event discrimination using subsets with different DTR from the rise time distributions (RTDs). Finally, we present the synergistic capability of metascintillators to enhance Cherenkov photons detection when used along with VUV-sensitive SiPMs.**

***Index Terms*—Bismuth Germanate (BGO), cherenkov, coincidence time resolution (CTR), EJ232, LYSO, metapixel, metascintillator, near-ultraviolet (NUV), silicon photomultiplier (SiPM), time-of-flight positron emission tomography (TOF-PET), vacuum-ultraviolet (VUV).**

Manuscript received 26 October 2022; revised 27 April 2023 and 28 June 2023; accepted 17 August 2023. Date of publication 31 August 2023; date of current version 3 November 2023. This work was supported in part by the European Research Council (ERC) under the European Union's Horizon 2020 Research and Innovation Program (4D-PET) under Grant 695536, and in part by the Brazilian Funding Agency Conselho Nacional de Desenvolvimento Científico e Tecnológico (CNPq) under Grant 202378/2020-9. *(Corresponding author: Riccardo Latella.)*

This work did not involve human subjects or animals in its research.

Riccardo Latella, Paul Lecoq, and Georgios Konstantinou are with the Metacrystal S.A., 1228 Geneva, Switzerland, and also with the Instituto de Instrumentacion para Imagen Molecular, Centro Mixto CSIC, Universitat Politècnica de València, 46022 Valencia, Spain (e-mail: riccardo@metacrystal.ch).

Antonio J. Gonzalez and José M. Benlloch are with the Instituto de Instrumentacion para Imagen Molecular, Centro Mixto CSIC, Universitat Politècnica de València, 46022 Valencia, Spain.

Daniel A. B. Bonifacio is with the Nuclear and Energy Research Institute (IPEN/CNEN), São Paulo 05508-000, Brazil, and also with the Instituto de Instrumentacion para Imagen Molecular, Centro Mixto CSIC, Universitat Politècnica de València, 46022 Valencia, Spain.

Miroslavna Kovylina and Amadeu Griol are with the Nanophotonics Technology Center, Universitat Politècnica de València, 46022 Valencia, Spain.

Color versions of one or more figures in this article are available at https://doi.org/10.1109/TRPMS.2023.3310581.

Digital Object Identifier 10.1109/TRPMS.2023.3310581

I. Introduction

HIGH-PRECISION time-of-flight positron emission tomography (TOF-PET) scanners could reach 10-ps FWHM coincidence time resolution (CTR) performance, as there is no physical barrier to this goal [1]. For this to happen, we need to look for new scintillating materials to overcome the limitations of the state-of-the-art LYSO. Along with that, a fast and low-noise electronic system plays a fundamental role in the reliability of the analysis and measurement as we approach CTR values below 100 ps [2].

Regardless of the emission type and wavelength, gamma-ray interactions generate an isotropic emission of photons in scintillating material which eventually impinge on the extraction surface with a specific angle [3]. According to Snell's law, each scintillation photon can reach the photodetector depending on the refractive indexes of the two materials at the interface of the extraction surface and its incidence angle.

Bismuth Germanate (BGO) crystals exhibit interesting characteristics, among which are the high density (7.13 g/cm^3), the high-attenuation length (1.10 cm at 511 keV), and the high-refractive index (2.15 @ 480 nm). Moreover, they produce scintillation photons with emission wavelengths between 370 and 640 nm. In addition, Cherenkov photons are also produced, and their wavelength dependency and transmittance are shown in Fig. 1. While Cherenkov wavelength is inversely proportional to the square of wavelength ($1/\lambda^2$), the self-absorption of BGO around 310 nm limits the extraction of Cherenkov photons [4].

An alternative method that allows for improvements in the performance of TOF-PET scanner technology is based on metascintillators. These are based on a new concept combining fast and high-density materials, exploiting the best characteristics of timing resolution and stopping power, respectively [6], [7], [8], [9], [10], [11].

The first generation of metascintillators has been thought to have no optical or coupling material between the thin layers of the two scintillation materials. Each plate is surrounded by a very thin layer of air with a refractive index of 1 for all relevant wavelengths [9]. The two materials share their gamma interaction energy through the recoil electron. Indeed, the trajectory of this particle can cross multiple times the two materials introducing the concept of energy-sharing (Fig. 2).

Until now, few works have tried to combine the added value of Cherenkov and metascintillator heterostructures [12], [13]. Moreover, an attempt has yet to be made to

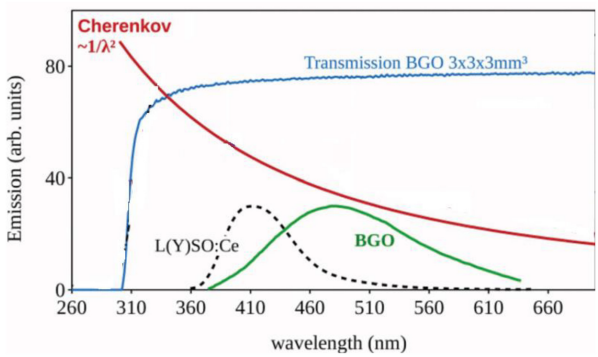

Fig. 1. Emission spectra of BGO, LYSO:Ce, and Cherenkov radiation compared to the BGO transmission. Modified from [5].

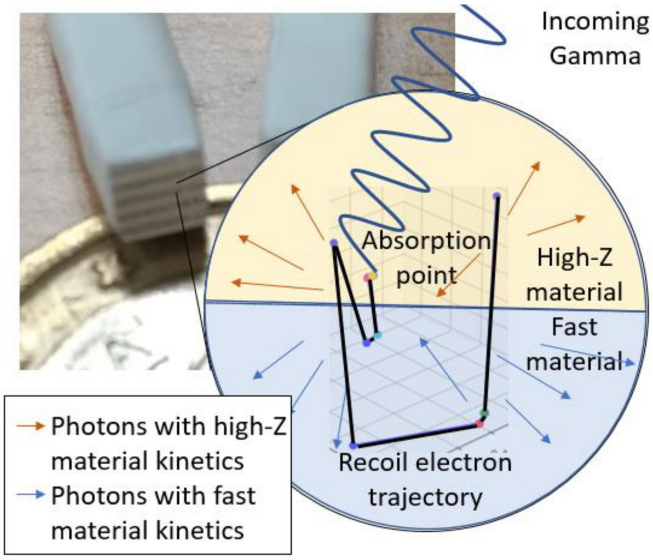

Fig. 2. Recoil trajectory and photon generation inside a metapixel [10].

channel BGO-produced Cherenkov photons through different materials.

This article summarizes the potential of timing using Cherenkov emissions in BGO through a novel technology. The results of the CTR measurements using silicon photomultipliers (SiPMs) from Fondazione Bruno Kessler (FBK) explicitly developed for measurements in the deep UV are presented. Furthermore, the effects of optical coupling materials on light extraction and the timing resolution have been evaluated. Finally, the capability to guide Cherenkov photons using the EJ232 plastic and their timing potential is considered.

II. Materials and Methods

A. Pixels: Bulk, Pseudo, and Meta

We have tested three types of pixels, namely, metapixels (m), made of two different scintillation materials, conventional bulk pixels (b) and the so-called pseudo pixels (p), formed by thin plates of the same material. Meta-pixels were built from BGO and EJ232 materials.

The reference detector crystal is a bulk 3×3×5-mm^3 LYSO:Ce,Ca from SIPAT (China). The 5-mm length for this pixel has been chosen to provide excellent detector time resolution (DTR) performance.

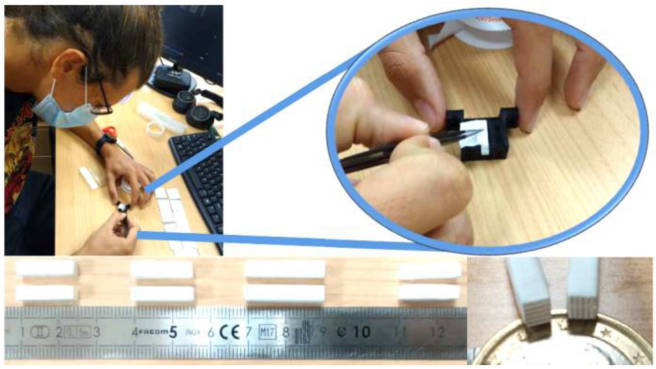

Fig. 3. (Top) Metapixel manufacturing process. (Bottom-left) Some of the metapixels in our disposal. (Bottom-right) Metapixel cross section with the two compound materials clearly distinguishable.

TABLE I
Pixels Characteristics

Pixel Name	Pixel Material(s)	Sizes	Effective Density
bLYSO	LYSO:Ce,Ca	3×3×5 mm^3	7.41 g/cm^3
bBGO	BGO	3×3×15 mm^3	7.13 g/cm^3
bEJ232	EJ232	3×3×15 mm^3	1.023 g/cm^3
pBGO1	BGO	3×3×15 mm^3	7.13 g/cm^3
pBGO2	BGO	3×3×15 mm^3	7.13 g/cm^3
pEJ232	EJ232	3×3×15 mm^3	1.023 g/cm^3
mBE	BGO/EJ232	3×3×15 mm^3	5.09 g/cm^3

Table I. Pixel type details. Every pixel has its own specific name.

Table I lists different custom-made bulk, pseudo, and meta-pixels. All these pixels have been covered with ESR plates and then wrapped in several layers of 0.075-mm Teflon to minimize the light losses due to the gap between the edge of the ESR film and mechanically stabilize the structured p and m pixels [14]. Two types of pseudo-BGO pixels have been compared, respectively, pBGO1 and pBGO2. The differences between these two pseudo pixels are the thickness of the BGO plates (0.3 mm for pBGO1 and 0.2 mm for pBGO2) and the treatment used for the thin lateral plate surfaces (unpolished for pBGO2 while polished for pBGO1). The large surfaces are polished for both cases. This decision has been made because the rough surfaces reduce the cost of every single plate and, therefore, the overall pseudo or meta pixel. For the 0.1-mm plates of pEJ232, the same surface treatment of pBGO2 has been used. For this reason, the metapixel tested in this work (mBE) is made by interleaving the plates of these two materials.

Fig. 3 shows the manufacturing process and some of the resulting metapixels.

B. Wavelength Sensitivity (SiPMs and Coupling Materials)

We used SiPMs from FBK, with the physical characteristics described in Table II [15]. The vacuum-ultraviolet (VUV) sensor is efficient to low wavelengths around 200 nm and, for this reason, has no protective layer on top of the silicon, as most

TABLE II
SiPM Characteristics

Type of SiPM	Chip Size	Cell Size	Voltage Breakdown
NUV-HD	3.1×3.2 mm^2	40 µm	32 V
VUV-HD	3.0×3.4 mm^2	35 µm	31.5 V

Table II. FBK SiPM details. More information about these devices can be found in [15].

industrially available materials compromise this sensitivity in the VUV region. The near-ultraviolet (NUV) SiPMs were also provided without this layer to compare the results. Therefore, these photosensors were very fragile. The bonding wire part has been covered by epoxy resin to make them slightly more robust. This has been observed to be very effective in terms of SiPM lifetime. For all SiPMs, a bias voltage scan was performed to find the best-operation point. While the diode sizes are slightly different, the built pixels are always smaller than that, covering the center of the SiPM.

The difficulty of finding suitable materials with limited absorption and reflection in the VUV region also stands for coupling materials. Moreover, most specifications refer to transparency over several centimeters, a different context than the few micrometers of the thickness of optical coupling placed between the scintillator and SiPM.

We tested two optical coupling materials: 1) bi-distilled glycerin (GL) and 2) SS-988 (SS), an optical grease from Silicone Solutions. In a previous paper [16], it was noticed that glycerin could deteriorate the SiPM.

Another drawback of glycerin is its viscosity. Since its melting/freezing point is at 17.8 °C, we avoided measurements at room temperature to prevent the liquid glycerin from dropping out of the SiPM area, getting absorbed by the Teflon around the crystal, damaging the SiPMs, or evaporating. Using SS-988, these effects were not visible, but this material is not a valid candidate for light transmittance on the deep UV. Even if VUV sensors produce similar results independently from which coupling material is used, we have decided to test our meta-pixel mBE with glycerin.

C. Measurements of Optical Characteristics of BGO

A Fourier-transform infrared (FTIR) system (Vertex 80 by Bruker, Billerica, MA, USA) outfitted with OPUS software was used to characterize the transmittance in the wavelength range of 250 to 500 nm. The spectrometer configuration for this range included a deuterium source, CaF_2 beamsplitter, preamplifier gain C, and RT-GaP Diode detector. Both source and sample apertures (6 and 1 mm in diameter, respectively), were employed. Another measurement feature included a 40 KHz low-pass filter and double-sided forward-backward acquisition mode. The resulting spectra were Fourier converted in OPUS using a phase resolution of 32 MHz/no peak search phase correction mode, Blackmann-Harris 3-term apodization function, and zero filling factor of 2. All spectra, including background measurements, were recorded at 4 cm^{-1} resolution and averaged using 128 scans.

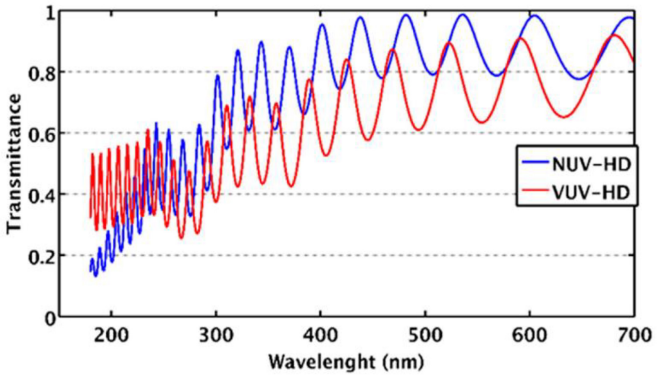

Fig. 4. Calculated transmittance in silicon of normal incident light on the near ultraviolet high-density antireflective coating (NUV-HD ARC, blue line) and on the modified ARC of VUV-HD SiPMs. Taken from [15].

We used this system to evaluate the absorption characteristics of BGO pieces of 0.2-mm thickness, such as the ones, used in the presented metapixels. This was done in comparison with standard 3×3-mm^2 area pieces. The range closer to 300 nm is particularly interesting for Cherenkov production due to the reduced wavelength and because BGO has a significantly higher-refractive index at these wavelengths [17]. The VUV SiPM has a slightly improved sensitivity compared to the NUV in the concerned area (Fig. 4).

D. Double Channel Readout Circuit

The front-end electronic board used in this work is based on previous publications [18] but with several specific redesigns for our current purposes. It is a double-channel readout circuit based on timing and energy channels. Fig. 5 top shows a simplified version of the read-out schematic.

In the balun-based differential readout path, the dual-stage amplifier has been reduced to a single time amplification stage (TAS) with broadband HMC311SC700-8-GHz amplifier to reduce the power consumption and the noise level (Fig. 5, middle-right) while maintaining possible to read the fast-rise time and the voltage drop across the SiPM without compromising timing performance. Notice that this has been achieved without any electromagnetic shielding. A specifically designed wideband Bias-T has been introduced to properly decouple the AC from the DC signal without losing significant frequency content. Indeed, the bandwidth frequency domain is limited by the balun (10 MHz) and the oscilloscope (8 GHz).

In the energy path, the unity voltage amplification stage composed of an EL5167 Operational Amplifier with a −3 dB bandwidth of 1.4 GHz provides the signal seen at the shunt resistor on the SiPM anode. The resulting boards are shown at the bottom side of Fig. 5.

E. Coincidence HF Setup

Our coincidence setup comprises a Na-22 radioactive source between two aligned gamma-ray detectors. Each detector consists of a scintillator that converts gamma rays into optical photons, a SiPM that transforms photons into electric current, and a front-end electronics board that extracts the electric

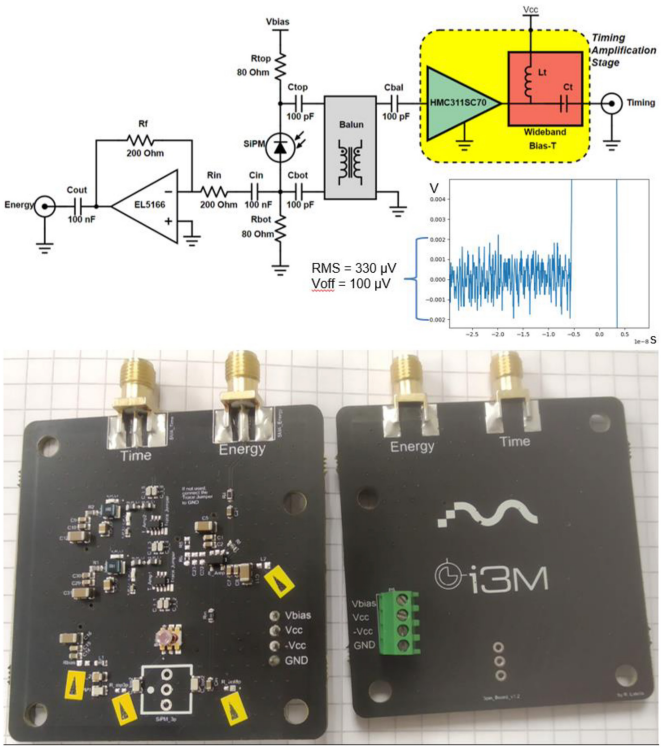

Fig. 5. (Top) schematics of the HF-amplifier readout electronics employing a timing amplification stage (TAS) composed of HMC311SC70 bipolar monolithic microwave integrated circuit (MMIC) amplifiers and a wideband Bias-T. (Top-right) A screenshot of the low noise from the timing signal. The RMS is calculated to be around 330 μV with a small offset of 100 μV. (Bottom) Front-end boards, (bottom-left) front side, and (bottom-right) back side.

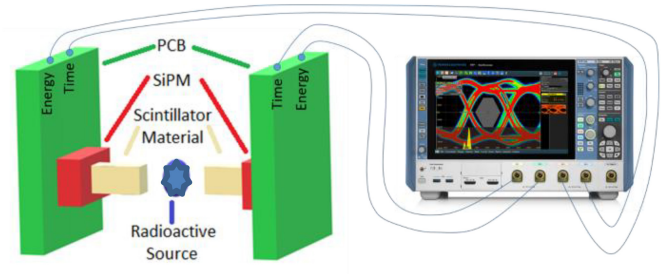

Fig. 6. Coincidence HF setup's sketch.

signal for further processing without significantly degrading the signal-to-noise ratio. At the end of this conversion chain, we used a high-performance 8-GHz bandwidth oscilloscope (Rhode & Schwarz RTP084) with four channels connected to each board's timing and energy channels (Fig. 6). To protect the coincidence setup from direct light and humidity, a 37-cm black cubic foam box has been filled with silica bags making small holes just for the supply cables, the oscilloscope probes, the temperature sensor, and the compressed cold air. The setup has been placed in a temperature-controlled environment at 14 °C–15 °C with variations below ±0.5 °C.

F. Event Filtering and Fitting Distribution

Coincidence filtering has been done directly on the oscilloscope by selecting events above a specific voltage threshold for each detector. By analyzing the maximum amplitude

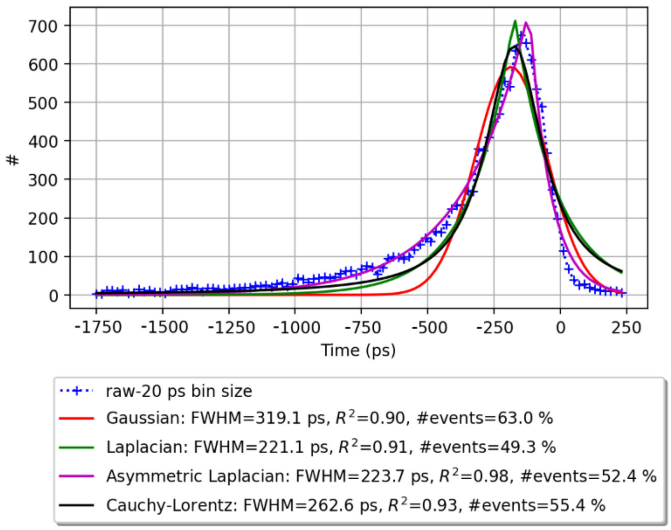

Fig. 7. Asymmetric distribution using bLYSO as reference detector and bBGO as tester with different fitting results. The maximum of the distribution is around −180 ps.

of the energy signal, it is possible to discern photoelectric events from Compton interactions. In the case of metapixels, this approach is not directly applicable, as the pulse height is a combination of energy shared between materials. Photoelectric events are improbable in plastic scintillators. Hence, the threshold chosen was the same as the BGO photopeak, allowing to discard of dark counts and low-energy events. Nevertheless, the events used to characterize plastic reach around 150-keV energy interactions.

Depending on the scintillator under test and the event selection, the Δt distributions might be Laplacian, Lorentzian, or a mixture of Gaussian functions [19]. Since all the measurements for this work are made against a reference crystal, most results show an asymmetric distribution, especially the ones with only BGO as testing material, as shown in Fig. 7.

The goodness of our fitting procedure was based on the regression-square value R^2. The regression predictions perfectly fit the data when R^2 is equal to 1. In addition, the true FWHM value has been added and calculated by simply taking the linear interpolation of the rising and falling half-maximum values. As an example, in Fig. 7, the asymmetric Laplacian fitting resulted in the best R^2. In order to find the true FWHM of the distribution, we perform the linear interpolation of the raw data. In this case, the true FWHM is 274.4 ps which includes 58.5% of the Δt distribution events. The DTR and intrinsic CTR (CTR_{INT}) of the tested pixels are then calculated from the expressions (1) and (2)

$$DTR_{TEST} = \sqrt{CTR^2 - DTR_{REF}^2} \tag{1}$$

$$CTR_{INT} = \sqrt{2} * DTR_{TEST}. \tag{2}$$

G. Detecting Cherenkov and Rise Time Distribution

The fast-rising edge of the timing channel refers to the constructive pile-up of detected photons and is used to detect and discriminate Cherenkov photons [12], [18], [20]. For the rise time distribution (RTD) analysis, we fixed the voltage

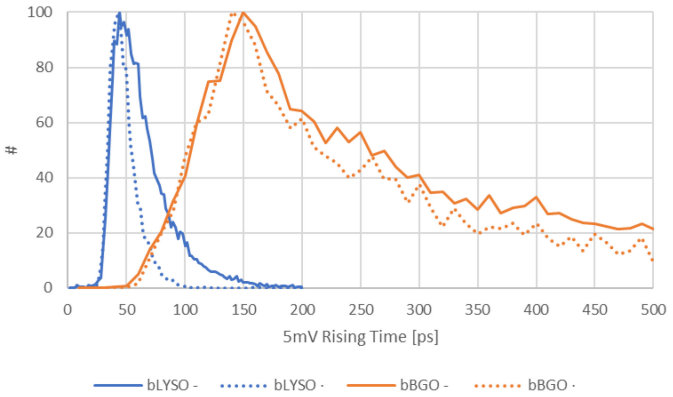

Fig. 8. Comparison RTD plots of bLYSO (in blue) and bBGO (orange) choosing cFS events (solid lines) and cPP events (doted lines). In both cases the sensor used is an NUV-HD coupled with SS.

threshold values just above the signal noise level at 3 and 8 mV.

Considering the equation of Cherenkov emission, many Cherenkov photons are produced below 300 nm, and a small amount of them is detectable with NUV SiPM. This occurs since BGO absorbs photons at this range [4]. However, in our meta-pixels, BGO is only 300 or 200-μm thin and combined with transparent materials to photons below 300 nm. This means that a VUV-sensitive sensor is expected to extract more Cherenkov photons from a metapixel than a NUV one. Moreover, it is possible to channel UV light through the air gap between the metalayers, enhancing the amount of Cherenkov photons collected in the deep UV region.

An essential feature of the metascintillators analysis is the ability to remove Compton's contributions. The photoelectric and Compton interactions are distinguishable for bulk pixels when plotting the energy spectrum. In metascintillators, especially where the two components have different light yields, the energy spectrum information needs to be combined with a distribution that can act as an energy-sharing surrogate [7], [8]. The RTD helps to understand which are the fastest events for the different contributions. Indeed, the RTD changes its profile depending on the events we consider. We focus on the coincidence Full Spectrum (cFS) and the coincidence Photopeak (cPP) RTDs, using the valley region in the energy spectrum to separate Compton from photoelectric events. The first considers all the events above a low threshold to avoid noise pollution, while the second is obtained by taking just photoelectric interactions. Fig. 8 shows the differences between the bLYSO and bBGO RTDs for all events (cFS) and just photoelectric interactions (cPP). With this rise time information, it is possible to filter just those events that are faster than a certain threshold. In this work, we have selected 100 ps as our rise time threshold, considering that pEJ232 has almost 100% of cPP events below this threshold. This will be shown in more detail in the Results section.

III. Results

A. Reference Detector Baseline Results

Two reference detectors ($3\times3\times5$-mm^3 LYSO:Ce,Ca coupled with the SS-988 to a NUV-HD SiPM) have been placed

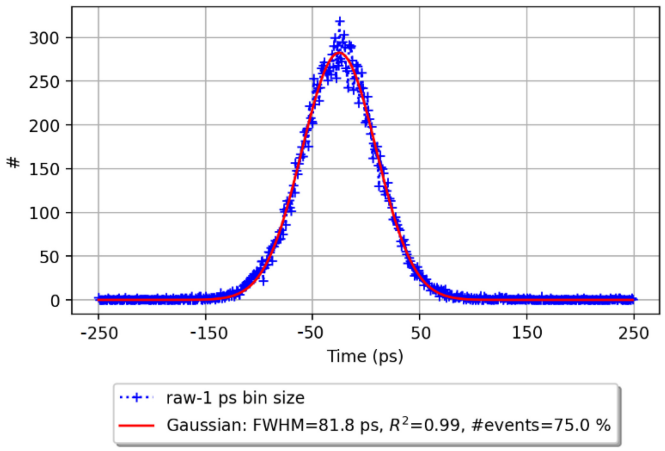

Fig. 9. CTR result of two bLYSO coupled with SS-988 to NUV-HD sensors.

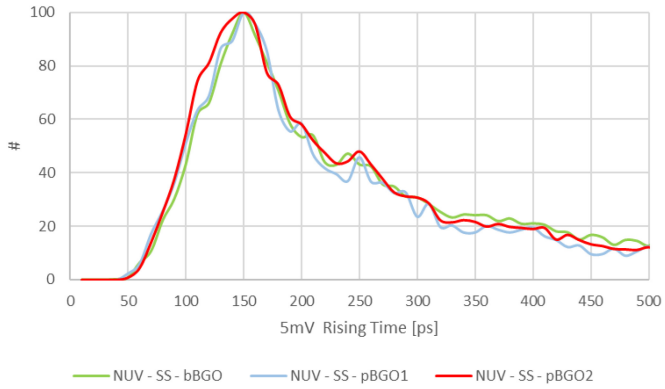

Fig. 10. RTD distributions of cPP events of bBGO, pBGO1, and pBGO2 coupled with SS-988 to NUV-HD sensors.

in coincidence, resulting in a CTR of 82 ps leading to a DTR of 58 ps (cPP), as shown in Fig. 9. The true FWHM is 75.9 ps which includes 70.3% of the Δt distribution events. In Fig. 8, the coincidence full-spectrum (cFS) and photopeak (cPP) RTDs of the reference detector are compared (blue lines, dotted and solid). By removing the Compton scattering interactions, the remaining events are the fastest ones.

B. From Bulk to Pseudo

In this section, the pixels have been tested with the NUV-HD sensor and SS-988 (SS) coupling material. Table III shows a slight CTR improvement in pBGO1 compared to bBGO, while pBGO2 presents a slightly worse CTR. Regarding the RTD of these three pixels, the difference in the distributions, as shown in Fig. 10, is within statistical margins, with the pBGO2 somewhat faster with around 5% fast events (below 150 ps) more than the other two distributions.

C. BGO/EJ232 Characterization

Table IV shows that the CTR of pEJ232 and mBE are comparable. This can be explained by the light-guiding concept previously discussed, where the fast Cherenkov photons of the BGO plates are now traveling through the EJ232 plates before being extracted. Moreover, because of the lack of photopeak region, the EJ232 CTR corresponds to all interactions

TABLE III
CTR RESULTS

Pixel	CTR [ps]	DTR [ps]	CTR_{INT} [ps]
bBGO	224 (269)	216	306
pBGO1	199 (251)	190	269
pBGO2	230 (247)	223	325

Table II. NUV-HD with SS-988 cPP results comparing bBGO, pBGO1 and pBGO2, using a NUV-HD LYSO:Ce,Ca reference detector. Between parenthesis, the CTR results using the true FWHM.

TABLE IV
CTR RESULTS

Pixel	CTR [ps]	DTR [ps]	CTR_{INT} [ps]
pEJ232	165 (174)	154	218
mBE	169 (208)	159	224

Table III. CTR results comparing NUV-HD pEJ232 and VUV-HD mBE, using a NUV-HD LYSO:Ce,Ca reference detector. Between parenthesis, the CTR results using the true FWHM.

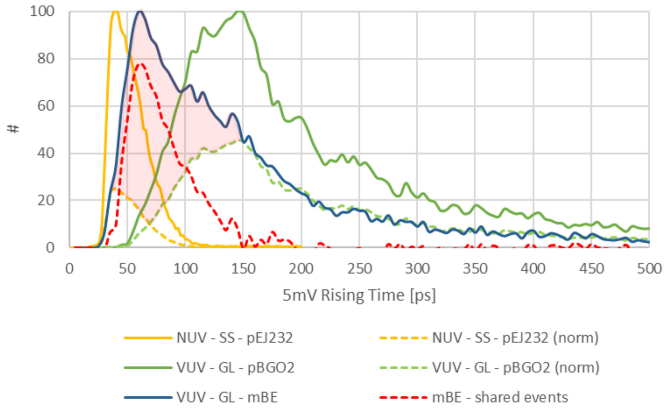

Fig. 11. RTD distributions of pEJ232 events coupled with SS to NUV-HD sensor (yellow line), and pBGO2 and mBE coupled with glycerin to VUV-HD sensor, (respectively, green, and blue lines). The solid lines are normalized by the maximum value of the relative distributions, while the yellow and green dashed ones are a normalized version of those with the same color. Finally, the dashed red line shows the projection of the red area containing only the shared mBE events.

having an energy above the Compton area of pBGO2. Hence, the timing results consider a part of those plastic scattering events.

Fig. 11 depicts the cPP RTDs for different materials and configurations for NUV and VUV photosensors. Here, it is visible the mBE, pEJ232, and pBGO2 RTDs and how the mBE (blue line) shares both material characteristics, especially having the same starting point of the pEJ232 (yellow line) and the events maximum in between the other two distributions. In this plot, it is possible to appreciate how the RTD can be used as an energy-sharing surrogate.

Moreover, it is possible to isolate shared events by normalizing the pEJ232 and pBGO2 lines, (respectively, yellow and green dashed lines of Fig. 11) to match the mBE RTD features. Indeed, in Fig. 11, the red dashed line is obtained by removing the normalized pseudo events from the overall metapixel contribution, showing the projection of the red area containing only the shared mBE events.

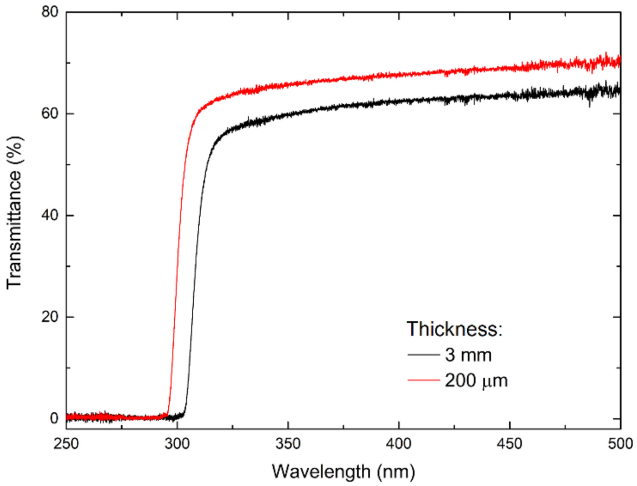

Fig. 12. FTIR transmittance measurement for BGO of different dimensions. There is significant difference at the area around 300 nm, which leads to an improvement of Cherenkov photon collection. Width and length of both samples is, respectively, 3 and 15 mm.

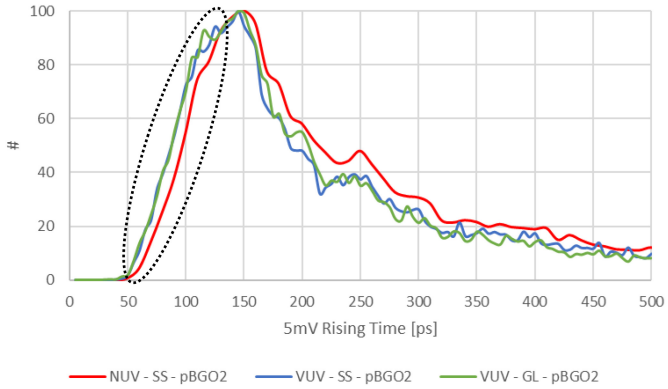

Fig. 13. RTD distributions of pBGO2 cPP events coupled with SS-988 and glycerin to NUV-HD and VUV-HD sensors. Highlighted in the black dotted oval, the difference in Cherenkov population between NUV-HD and VUV-HD

D. Absorption Dependence of BGO Geometry

The FTIR spectroscopy experiment has provided wavelength-dependent absorption values for BGO pieces of 0.2-mm thickness (Fig. 12). Compared to the standard 3-mm BGO thickness, we observe a significant improvement in transmission. Cherenkov light at this range is more likely to be extracted from crystals cut in thin configurations. This synergizes with the improved PDE of the VUV at those wavelengths and the improved Cherenkov production due to lower-wavelength and higher-refractive index of BGO around 300 nm.

E. Coupling Material and Cherenkov Populations

To test the possible improvements with VUV-HD sensors for Cherenkov photon extraction, we tested the pBGO2 pseudo-pixel using both SS-988 and glycerin and compared it with NUV acquisition. The results show no significant difference in terms of CTR, less than a 10-ps difference. In contrast, the RTDs show an increment in the fast side of the distribution,

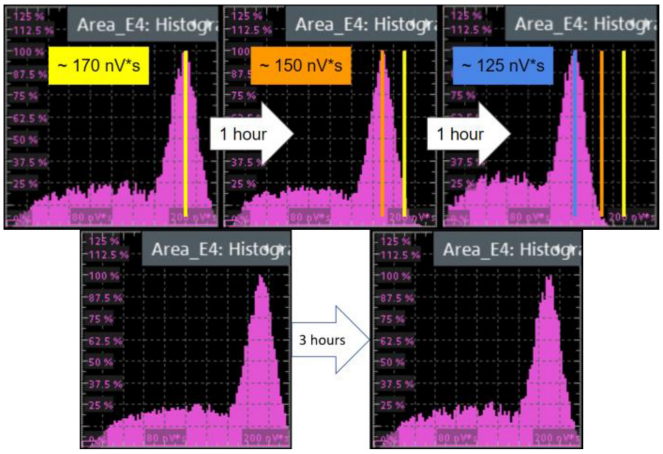

Fig. 14. Energy profiles of bBGO pixel. (Top) cFS plots at different time intervals. Glycerin was used at room temperature for this test (25 °C). (Bottom) on the left the cFS, on the right the coincidence spectrum after filtering the fast events with rise time below 100 ps. Both using glycerin at temperature below 18 °C.

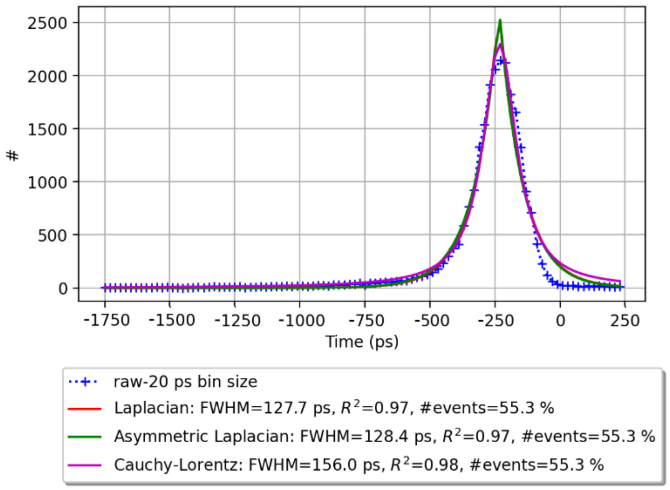

Fig. 15. CTR result of mBE couple with glycerin to a VUV-HD sensors and filtering just those events that are faster than 100 ps of the RTD distribution.

where the events with significant Cherenkov photon population are found (Fig. 13, black dotted oval). This might also be caused by the small differences between SiPMs.

Both coupling materials showed a largely similar behavior when considering the RTD; however, when using glycerin at room temperature, the gain of the energy profile was significantly decreased in less than an hour (Fig. 14, top). After reducing the temperature below 15 °C and minimizing the amount of glycerin, the energy spectrum became stable (Fig. 14, bottom).

This has been tested to be efficient also considering that glycerol has its melting point at 17.8 °C, in this way, reducing the viscosity of the material. At the same time, when comparing the RTDs of BGO with different coupling materials and SiPMs, we see a significant improvement when using VUV. However, using glycerin or regular grease does not change the RTD significantly.

F. Isolating Fast Datasets

If we consider only those fast events that occur below the 100-ps RT threshold, we obtain that the percentages of events are:

1) 97.7% for pEJ232;
2) 11.8% for pBGO;
3) 42.1% for mBE.

Considering that almost 100% of all pEJ232 events are already below 100 ps of 5 mV RTD, we can assume that the CTR will stay the same, while for pBGO2 and mBE would not be the case. This means that for almost 50% of all the mBE photoelectric interactions, we can further improve the CTR by selecting a fast subset of events. Indeed, the CTR of mBE using this rise time filtering approach is 156 ps, even better than the pEJ232 result (Fig. 15) The true FWHM is 184.9 ps which includes 66.3% of the Δt distribution events. This last result is instead a bit over the best result achieved with pEJ232 (174 ps), though really close, indicating that the BGO Cerenkov photons almost entirely drive the timing resolution.

IV. Discussion

In this work, we have isolated subsets of 511-keV annihilation photon events to demonstrate how the pileup of optical photons, which provides the best timing, can be done with the combination of Cherenkov and fast-metascintillator photons. However, the demonstration of increased sensitivity, even for materials without emission in the VUV, leads to further investigation of a potential synergy of those timing mechanisms.

Minor CTR improvements have been observed between pBGO1 and bBGO, while pBGO2 presents a slightly worse CTR (not if we consider the true FWHM result). This can be attributed to the unpolished thin surfaces of pBGO2. Indeed, the extracted light must pass through a rough surface, compromising the light collection. This is an exciting result since pBGO2 and bBGO CTRs are substantially identical.

Considering the use of glycerin as a coupling material, we have observed the formation of a black powder on top of the SiPM. Initially, the cause of this phenomenon was attributed to some oxidation in a metal part of the SiPM. Further investigations have determined that glycerin creates a conductive bridge between the anode and cathode bonding wires. By applying a voltage over the breakdown point of the SiPM, the current might flow through the glycerin producing an electrochemical reaction.

By comparing the RTD of different materials, we demonstrate that the RTD using a 5-mV threshold for the rise time can be used as an energy-sharing surrogate. This is significant as the RTD is commonly used for Cherenkov photons discrimination [5], [16], [18], allowing a single tool to be applied for all fast-timing mechanisms.

Using the RTD for event discrimination has revealed datasets with variable CTR and allowed feature matching of distributions of bulk materials, in this case, BGO and EJ232. The RTD approach seems to be well applicable to the metascintillator case, allowing the characterization of events according to their energy sharing. When comparing the RTD of bulk BGO, including Cherenkov and metascintillators, we

see that in the second case, a significantly higher population of events is found in the favorable fast area of this distribution.

From the comparison between VUV and NUV read-outs, a better-Cherenkov event population is gathered with VUV SiPM as a percentage of the whole acquisition. This might also be caused by the small differences between SiPMs. Further investigation is needed. The same can be said by comparing bulk (b) and laminated (p) pixels. As all other possibilities have been eliminated, we can assume that laminated scintillators with VUV SiPM improve Cherenkov photon extraction, as demonstrated in the presented FTIR measurements. This leads to a synergistic effect supporting using metascintillators for improved Cherenkov photon detection. An interesting artifact was observed below 250 nm, hinting at a potential second transmissive band for BGO. Detailed measurements will take place and be presented in different works.

Concerning the fitting methods used for the Δt distributions, we decided to have as best fit the one determined by the highest-regression-square value R^2. We use the asymmetric Laplacian fit for asymmetric distribution because most events are in the long tail of BGO timing contributions. This is also why we use a very fast reference detector. In this way, the error contribution introduced when recalculating the DTR using different fitting methods can be considered negligible. Additionally, the true FWHM calculated by linear interpolation is presented for each timing spectrum.

We observed that the CTR results for pBGO2 were comparable even when changing photosensors and coupling materials. Thinking about a metapixel composed of pBGO2 and pEJ232 plates, we would expect timing performances between one of these two pseudo-pixels. Indeed, the results show this but with a strong presence of shared events pushing the CTR of mBE to be very close to the one of pEJ232.

These results can be further improved using fully polished plates of BGO material and some post-processing techniques, like time-walk correction [8]. However, this work aims to demonstrate that it is possible to isolate and explain the distributions of CTR for events of different natures directly at the oscilloscope without any post-processing.

Further analysis will be conducted on the combination of slabs of various thicknesses, exploiting the characteristics of both materials. Nevertheless, we demonstrated here that using both metascintillators and Cherenkov timing mechanisms in the same acquisition and isolating the faster events is possible. As it has been demonstrated that variable depth-of-interaction is one of the primary mechanisms deteriorating the CTR of scintillators, we are working on developing metascintillators that include precise DOI characterization [21], [22], [23]. This information will be combined with the energy sharing and first photon-arrival through neural networks to improve all metascintillator specifications collectively, according to recently published works [24].

V. Conclusion

In this work, we demonstrate that the combined use of VUV-sensitive SiPM technology, along with VUV transparent or semi-transparent optical couplings and scintillator heterostructures, can improve Cherenkov photon detection. We also showed how the metascintillator and Cherenkov approaches for fast timing could complement each other. This enhanced the occurrence of prompt photons and consequent IPTD, a strong indicator of improved CTR for selected event subsets. We have also demonstrated that the RTD can be a helpful tool, along with the energy spectrum, for the characterization of fast events in metascintillators, as it allows easy and direct selection of faster or more shared events. Moreover, we show that the features of pulses between bulk BGO and EJ232 materials can be directly isolated from the metascintillator distribution.

By splitting the shared photoelectric interactions almost in half (42%) with a rise-time filter of 100 ps, we show that the faster part of the mBE events has a CTR of 156 ps (184 ps using the true FWHM), comparable to the CTR of only plastic scintillators, but with significantly improved stopping power due to the presence of a high-Z material, such as the BGO and the inclusion in this fast dataset of the Cherenkov-timed events. These teachings can be used for future metascintillator analysis and in the case of metascintillators, where one of the materials contributes to good timing through the presence of Cherenkov photons.

Acknowledgment

This concept has been initiated in the frame of the ERC Advanced Grant TICAL #338953, PI Paul Lecoq, and the related Prof-of-Concept Project ULTIMA #680552, both funded by the European Commission. It has been in part supported by the European Research Council (ERC) under the European Union's Horizon 2020 Research and Innovation Program (Grant Agreement #695536) and the Brazilian funding agency Conselho Nacional de Desenvolvimento Científico e Tecnológico (CNPq, Grant Agreement No 202378/2020-9). It is pursued through a public–private partnership between Multiwave Metacrystal SA, Geneva, Switzerland, and the Instituto de Instrumentación para Imagen Molecular, Centro Mixto CSIC-UPV, Valencia, Spain. Their support is greatly acknowledged.

All authors declare that they have no known conflicts of interest in terms of competing for financial interests or personal relationships that could have an influence or are relevant to the work reported in this article.

Special thanks are given to Nicolaus Kratochwil and Fiammetta Pagano from CERN for their external review and help. Additional thanks are given to Maria Ruzzarin and Stefano Merzi from FBK.

References

[1] P. Lecoq, "Pushing the limits in time-of-flight PET imaging," *IEEE Trans. Radiat. Plasma Med. Sci.*, vol. 1, no. 6, pp. 473–485, Nov. 2017.

[2] J. W. Cates and C. S. Levin, "Evaluation of a TOF-PET detector design that achieves ≤ 100 ps coincidence time resolution," in *Proc. IEEE Nucl. Sci. Symp. and Med. Imag. Conf. (NSS/MIC)*, 2017, pp. 1–3, doi: 10.1109/NSSMIC.2017.8532998.

[3] P. Lecoq et al., "Progress on photonic crystals," in *Proc. IEEE Nucl. Sci. Symp. Med. Imag. Conf. (NSS/MIC)*, 2010, pp. 1970–1975, doi: 10.1109/NSSMIC.2010.5874119.

[4] P. Petkova, V. Marinova, T. Dimov, I. Iliev, and M. Gospodinov, "Magneto-optical effect in $Bi_4Ge_3O_{12}$ single crystals doped with vanadium," *J. Optoelectron. Adv. Mater.*, vol. 7, no. 1, pp. 439–442, 2005.

[5] S. Gundacker et al., "Experimental time resolution limits of modern SiPMs and TOF-PET detectors exploring different scintillators and Cherenkov emission," *Phys. Med. Biol.*, vol. 65, Jan. 2020, Art. no. 25001. [Online]. Available: https://doi.org/10.1088/1361-6560/ab63b4

[6] S. E. Brunner, L. Gruber, J. Marton, K. Suzuki, and A. Hirtl, "New approaches for improvement of TOF-PET," *Nucl. Instrum. Methods Phys. Res. Section A, Accel., Spectrometers, Detect. Assoc. Equip.*, vol. 732, Dec. 2013, pp. 560–563, doi: 10.1016/j.nima.2013.05.028.

[7] G. Konstantinou et al., "Metascintillator pulse feature and shape analysis to detect photoelectric interactions and energy sharing," in *Proc. IEEE Nucl. Sci. Symp. Med. Imag. Conf. (NSS/MIC)*, 2021, pp. 1–4.

[8] G. Konstantinou, P. Lecoq, J. M. Benlloch, and A. J. Gonzalez, "Metascintillators for ultrafast gamma detectors: A review of current state and future perspectives," *IEEE Trans. Radiat. Plasma Med. Sci.*, vol. 6, no. 1, pp. 5–15, Jan. 2022, doi: 10.1109/TRPMS.2021.3069624.

[9] P. Lecoq et al., "Metascintillators: New results for TOF-PET applications," *IEEE Trans. Radiat. Plasma Med. Sci.*, vol. 6, no. 5, pp. 510–516, May 2022, doi: 10.1109/TRPMS.2022.3161473.

[10] G. Konstantinou et al., "A proof-of-concept of cross-luminescent metascintillators: Testing results on a BGO-BaF2 metapixel," *Phys. Med. Biol.*, vol. 68, no. 2, 2023, Art. no. 25018.

[11] P. Mohr et al., "Image reconstruction analysis for positron emission tomography with heterostructured scintillators," *IEEE Trans. Radiat. Plasma Med. Sci.*, vol. 7, no. 1, pp. 41–51, Jan. 2023, doi: 10.1109/TRPMS.2022.3208615.

[12] R. M. Turtos, S. Gundacker, E. Auffray, and P. Lecoq, "Towards a metamaterial approach for fast timing in PET: Experimental proof-of-concept," *Phys. Med. Biol.*, vol. 64, no. 18, Sep. 2019, Art. no. 185018, doi: 10.1088/1361-6560/ab18b3.

[13] F. Pagano, N. Kratochwil, M. Salomoni, M. Pizzichemi, M. Paganoni, and E. Auffray, "Advances in heterostructured scintillators: Toward a new generation of detectors for TOF-PET," *Phys. Med. Biol.*, vol. 67, no. 13, 2022, Art. no. 135010, doi: 10.1088/1361-6560/ac72ee.

[14] H. Leem, Y. Choi, J. Jung, K. Park, Y. Kim, and J. H. Jung, "Optimized TOF-PET detector using scintillation crystal array for brain imaging," *Nucl. Eng. Technol.*, vol. 54, no. 7, pp. 2592–2598, 2022, doi: 10.1016/j.net.2022.02.009.

[15] A. Gola et al., "NUV-sensitive silicon photomultiplier technologies developed at Fondazione Bruno Kessler," *Sensors*, vol. 19, no. 2, p. 308, 2019, doi: 10.3390/s19020308.

[16] S. Gundacker et al., "VUV-SiPMs applied to BaF 2 cross-luminescence detection for high-rate ultrafast timing applications," *Phys. Med. Biol.*, vol. 66, no. 11, 2021, Art. no. 114002, doi: 10.1088/1361-6560/abf476.

[17] P. A. Williams, A. H. Rose, K. S. Lee, D. C. Conrad, G. W. Day, and P. D. Hale, "Optical, thermo-optic, electro-optic, and photoelastic properties of bismuth germanate (Bi4Ge3O12)," *Appl. Opt.*, vol. 35, no. 19, pp. 3562–3569, 1996.

[18] R. Latella, A. J. Gonzalez, J. Barrio, J. M. Benlloch, P. Lecoq, and G. Konstantinou, "Test setup and data selection protocols for the measurement of metascintillator CTR," *IEEE Trans. Radiat. Plasma Med. Sci.*, submitted to publication.

[19] N. Efthimiou et al., "TOF-PET image reconstruction with multiple timing kernels applied on Cherenkov radiation in BGO," *IEEE Trans. Radiat. Plasma Med. Sci.*, vol. 5, no. 5, pp. 703–711, Sep. 2020, doi: 10.1109/trpms.2020.3048642.

[20] N. Kratochwil, S. Gundacker, P. Lecoq, and E. Auffray, "Pushing Cherenkov PET with BGO via coincidence time resolution classification and correction," *Phys. Med. Biol.*, vol. 65, no. 11, 2020, Art. no. 115004, doi: 10.1088/1361-6560/ab87f9

[21] A. Gonzalez-Montoro et al., "Evolution of PET detectors and event positioning algorithms using monolithic scintillation crystals," *IEEE Trans. Radiat. Plasma Med. Sci.*, vol. 5, no. 3, pp. 282–305, May 2021, doi: 10.1109/TRPMS.2021.3059181.

[22] J. Barrio et al., "PET detector based on a semi-monolithic crystal with DOI and TOF capabilities," in *Proc. IEEE Nucl. Sci. Symp. Med. Imag. Conf. (NSS/MIC)*, 2020, pp. 1–3, doi: 10.1109/NSS/MIC42677.2020.9508047.

[23] M. Freire, A. Gonzalez-Montoro, F. Sanchez, J. M. Benlloch, and A. J. Gonzalez, "Calibration of gamma ray impacts in monolithic-based detectors using Voronoi diagrams," *IEEE Trans. Radiat. Plasma Med. Sci.*, vol. 4, no. 3, pp. 350–360, May 2020, doi: 10.1109/TRPMS.2019.2947716.

[24] M. Freire, S. Echegoyen, A. Gonzalez-Montoro, F. Sanchez, and A. J. Gonzalez, "Performance evaluation of side-by-side optically coupled monolithic LYSO crystals," *Med. Phys.*, vol. 49, no. 8, pp. 5616–5626, 2022, doi: 10.1002/mp.15792.